

The flavor transition process $b \rightarrow s\gamma$ in the $U(1)_X$ SSM with the mass insertion approximation

Xin-Xin Long^{1,2,3}, Shu-Min Zhao^{1,2,3*}, Xi Wang^{1,2,3}, Yi-Tong Wang^{1,2,3},
Tong-Tong Wang^{1,2,3}, Jian-Bin Chen⁴, Hai-Bin Zhang^{1,2,3}, Tai-Fu Feng^{1,2,3,5}

¹ *Department of Physics, Hebei University, Baoding 071002, China*

² *Key Laboratory of High-precision Computation and Application of Quantum Field Theory of Hebei Province, Baoding 071002, China*

³ *Research Center for Computational Physics of Hebei Province, Baoding 071002, China*

⁴ *College of Physics and Optoelectronic Engineering,*

Taiyuan University of Technology, Taiyuan 030024, China and

⁵ *Department of Physics, Chongqing University, Chongqing 401331, China*

(Dated: July 6, 2023)

Abstract

People extend the MSSM with the local gauge group $U(1)_X$ to obtain the $U(1)_X$ SSM. In the framework of the $U(1)_X$ SSM, we study the flavor transition process $b \rightarrow s\gamma$ with the mass insertion approximation (MIA). By the MIA method and some reasonable parameter assumptions, we can intuitively find the parameters that have obvious effect on the analytic results of the flavor transition process $b \rightarrow s\gamma$. By means of the influences of different sensitive parameters, we can obtain reasonable results to better fit the experimental data.

PACS numbers:

Keywords: $U(1)_X$ SSM, flavor transition, mass insertion approximation

* zhaosm@hbu.edu.cn

I. INTRODUCTION

The rare decay $\bar{B} \rightarrow X_s \gamma$ is the Flavor Changing Neutral Current (FCNC) process with great research value, whose CP averaged branching ratio is used to constrain many models of new physics. People have conducted multi-angle research on the process. The authors of Refs. [1–3] present the calculation of the rate of the inclusive decay $\bar{B} \rightarrow X_s \gamma$ in the two-Higgs doublet model (THDM). The supersymmetric effect on $\bar{B} \rightarrow X_s \gamma$ is discussed in Refs. [4–9].

Since the influence of new physics on FCNC process is mainly derived from the loop diagrams process, the decay process $b \rightarrow s \gamma$ is very sensitive to new physics beyond the Standard Model (SM). The average experimental data on the branching ratio of the inclusive $\bar{B} \rightarrow X_s \gamma$ is [10]

$$BR(\bar{B} \rightarrow X_s \gamma)_{exp} = (3.40 \pm 0.21) \times 10^{-4}, \quad (1)$$

and the prediction of SM at next-next-to-leading order (NNLO) is [11–18]

$$BR(\bar{B} \rightarrow X_s \gamma)_{SM} = (3.36 \pm 0.23) \times 10^{-4}. \quad (2)$$

A famous extension of the SM is the minimal supersymmetric extension of the standard model (MSSM) [19]. As a popular extension, the MSSM solves many problems. However, the explanation of neutrino oscillation requires tiny neutrino mass, which can not be naturally generated by the MSSM. So people extend the MSSM into multiple models, among which, the $U(1)_X$ extension of the MSSM is called as the $U(1)_X$ S SM [20, 21] with the local gauge group $SU(3)_C \otimes SU(2)_L \otimes U(1)_Y \otimes U(1)_X$. Compared to the MSSM, the $U(1)_X$ S SM has more superfields such as right-handed neutrinos. The right-handed neutrinos and the added Higgs singlets can explain the tiny mass of neutrino. It can alleviate the μ problem of the MSSM, because $\mu \hat{H}_u \hat{H}_d$ and $\lambda_H \hat{S} \hat{H}_u \hat{H}_d$ in the $U(1)_X$ S SM produce the effective $\mu'_H = \mu + \lambda_H v_S / \sqrt{2}$. Mixing the CP-even parts of H_d , H_u , η , $\bar{\eta}$, S can improve the masses of the tree-level lightest and sub-lightest CP-even Higgs particles.

The mass eigenstate basis is the most commonly used method in FCNC research. However, the mass eigenstate method depends on the mass eigenvalues of particles and rotation matrices, which makes it difficult to find the sensitive parameters clearly and intuitively. To solve this problem, we use another method - Mass Insertion Approximation (MIA) [21–25].

The MIA results can be alternatively obtained from expanding properly the expressions in the mass eigenstate basis [26]. At the analytical level, it avoids tedious calculations and reduces the chances of errors. In addition, its relatively concise and clear analytical results are helpful for the analysis of sensitive parameters.

To sum up, we investigate the FCNC process $b \rightarrow s\gamma$ under the $U(1)_X$ SSM by MIA. Our paper is organized as follows. In Sec.II, we mainly introduce the $U(1)_X$ SSM including its superpotential and the general soft breaking terms. The analytic expressions for $b \rightarrow s\gamma$ decay in the $U(1)_X$ SSM are given in Sec.III. In Sec.IV, we give the numerical analysis. And our conclusions are summarized in Sec.V.

II. THE $U(1)_X$ SSM

We extend the MSSM with the local gauge group $U(1)_X$ to obtain the $U(1)_X$ SSM, whose local gauge group is $SU(3)_C \otimes SU(2)_L \otimes U(1)_Y \otimes U(1)_X$. There are new superfields in it compared to the MSSM, including three Higgs singlets $\hat{\eta}$, $\hat{\bar{\eta}}$, \hat{S} and right-handed neutrinos $\hat{\nu}_i$. The $U(1)_X$ SSM has several advantages than the MSSM. For example, through the seesaw mechanism, light neutrinos obtain tiny masses at the tree level. The superpotential of this model is:

$$\begin{aligned}
W = & l_W \hat{S} + \mu \hat{H}_u \hat{H}_d + M_S \hat{S} \hat{S} - Y_d \hat{d} \hat{q} \hat{H}_d - Y_e \hat{e} \hat{l} \hat{H}_d + \lambda_H \hat{S} \hat{H}_u \hat{H}_d \\
& + \lambda_C \hat{S} \hat{\eta} \hat{\eta} + \frac{\kappa}{3} \hat{S} \hat{S} \hat{S} + Y_u \hat{u} \hat{q} \hat{H}_u + Y_X \hat{\nu} \hat{\eta} \hat{\nu} + Y_\nu \hat{\nu} \hat{l} \hat{H}_u.
\end{aligned} \tag{3}$$

We show the explicit forms of two Higgs doublets and three Higgs singlets here

$$\begin{aligned}
H_u = & \begin{pmatrix} H_u^+ \\ \frac{1}{\sqrt{2}}(v_u + H_u^0 + iP_u^0) \end{pmatrix}, & H_d = & \begin{pmatrix} \frac{1}{\sqrt{2}}(v_d + H_d^0 + iP_d^0) \\ H_d^- \end{pmatrix}, \\
\eta = & \frac{1}{\sqrt{2}}(v_\eta + \phi_\eta^0 + iP_\eta^0), & \bar{\eta} = & \frac{1}{\sqrt{2}}(v_{\bar{\eta}} + \phi_{\bar{\eta}}^0 + iP_{\bar{\eta}}^0), \\
S = & \frac{1}{\sqrt{2}}(v_S + \phi_S^0 + iP_S^0).
\end{aligned} \tag{4}$$

In Eq.(4), v_u , v_d , v_η , $v_{\bar{\eta}}$ and v_S respectively represent the vacuum expectation values(VEVs) of the Higgs superfields H_u , H_d , η , $\bar{\eta}$ and S . And two angles are defined as $\tan \beta = v_u/v_d$ and $\tan \beta_\eta = v_{\bar{\eta}}/v_\eta$.

The soft SUSY breaking terms of this model are shown as

$$\begin{aligned}
\mathcal{L}_{soft} = & \mathcal{L}_{soft}^{MSSM} - B_S S^2 - L_S S - \frac{T_\kappa}{3} S^3 - T_{\lambda_C} S \eta \bar{\eta} + \epsilon_{ij} T_{\lambda_H} S H_d^i H_u^j \\
& - T_X^{IJ} \bar{\eta} \tilde{\nu}_R^{*I} \tilde{\nu}_R^{*J} + \epsilon_{ij} T_\nu^{IJ} H_u^i \tilde{\nu}_R^{*I} \tilde{l}_j^J - m_\eta^2 |\eta|^2 - m_{\bar{\eta}}^2 |\bar{\eta}|^2 - m_S^2 S^2 \\
& - (m_{\tilde{\nu}_R}^2)^{IJ} \tilde{\nu}_R^{*I} \tilde{\nu}_R^J - \frac{1}{2} \left(M_X \lambda_{\tilde{X}}^2 + 2M_{BB'} \lambda_{\tilde{B}} \lambda_{\tilde{X}} \right) + h.c. \quad .
\end{aligned} \tag{5}$$

$\mathcal{L}_{soft}^{MSSM}$ represent the soft breaking terms of MSSM. In the $U(1)_X$ SSM, a new effect never seen in the MSSM occurs: the gauge kinetic mixing produced by the two Abelian groups $U(1)_Y$ and $U(1)_X$. In general, the covariant derivatives of $U(1)_X$ SSM can be written as [27–30]

$$D_\mu = \partial_\mu - i \begin{pmatrix} Y & X \end{pmatrix} \begin{pmatrix} g_Y & g'_{YX} \\ g'_{XY} & g'_X \end{pmatrix} \begin{pmatrix} A_\mu^Y \\ A_\mu^X \end{pmatrix} . \tag{6}$$

Under the condition that the two Abelian gauge groups are not broken, we can change the basis of the above equation by rotation matrix R , with A_μ^Y and A_μ^X representing the gauge fields of $U(1)_Y$ and $U(1)_X$ respectively,

$$D_\mu = \partial_\mu - i \begin{pmatrix} Y^Y & Y^X \end{pmatrix} \begin{pmatrix} g_Y & g'_{YX} \\ g'_{XY} & g'_X \end{pmatrix} R^T R \begin{pmatrix} A_\mu^Y \\ A_\mu^X \end{pmatrix} . \tag{7}$$

Then combined with our redefined

$$\begin{pmatrix} g_Y & g'_{YX} \\ g'_{XY} & g'_X \end{pmatrix} R^T = \begin{pmatrix} g_1 & g_{YX} \\ 0 & g_X \end{pmatrix} \text{ and } R \begin{pmatrix} A_\mu^Y \\ A_\mu^X \end{pmatrix} = \begin{pmatrix} A_\mu^Y \\ A_\mu^X \end{pmatrix} , \tag{8}$$

we get the covariant derivatives of the $U(1)_X$ SSM that changes the base:

$$D_\mu = \partial_\mu - i \begin{pmatrix} Y^Y & Y^X \end{pmatrix} \begin{pmatrix} g_1 & g_{YX} \\ 0 & g_X \end{pmatrix} \begin{pmatrix} A_\mu^Y \\ A_\mu^X \end{pmatrix} . \tag{9}$$

Three neutral gauge bosons A_μ^X , A_μ^Y and V_μ^3 mix together at the tree level, whose mass matrix is shown in the basis $(A_\mu^Y, V_\mu^3, A_\mu^X)$

$$\begin{pmatrix} \frac{1}{8} g_1^2 v^2 & -\frac{1}{8} g_1 g_2 v^2 & \frac{1}{8} g_1 (g_{YX} + g_X) v^2 \\ -\frac{1}{8} g_1 g_2 v^2 & \frac{1}{8} g_2^2 v^2 & -\frac{1}{8} g_2 g_{YX} v^2 \\ \frac{1}{8} g_1 (g_{YX} + g_X) v^2 & -\frac{1}{8} g_2 (g_{YX} + g_X) v^2 & \frac{1}{8} (g_{YX} + g_X)^2 v^2 + \frac{1}{8} g_X^2 \xi^2 \end{pmatrix} , \tag{10}$$

with $v^2 = v_u^2 + v_d^2$ and $\xi^2 = v_\eta^2 + v_{\bar{\eta}}^2$.

To get mass eigenvalues of the matrix in Eq.(10), we use two mixing angles θ_W and θ'_W . θ_W is the Weinberg angle and the new mixing angle θ'_W is defined by the following formula

$$\sin^2 \theta'_W = \frac{1}{2} - \frac{[(g_{YX} + g_X)^2 - g_1^2 - g_2^2]v^2 + 4g_X^2\xi^2}{2\sqrt{[(g_{YX} + g_X)^2 + g_1^2 + g_2^2]^2v^4 + 8g_X^2[(g_{YX} + g_X)^2 - g_1^2 - g_2^2]v^2\xi^2 + 16g_X^4\xi^4}}. \quad (11)$$

θ'_W appears in the couplings involving Z and Z' . The exact eigenvalues of Eq.(10) are deduced

$$\begin{aligned} m_\gamma^2 &= 0, \\ m_{Z,Z'}^2 &= \frac{1}{8} \left([g_1^2 + g_2^2 + (g_{YX} + g_X)^2]v^2 + 4g_X^2\xi^2 \right. \\ &\quad \left. \mp \sqrt{[g_1^2 + g_2^2 + (g_{YX} + g_X)^2]^2v^4 + 8[(g_{YX} + g_X)^2 - g_1^2 - g_2^2]g_X^2v^2\xi^2 + 16g_X^4\xi^4} \right). \quad (12) \end{aligned}$$

The other used mass matrices can be found in the works [31, 32].

In addition, there are some couplings that need to be used later:

$$\mathcal{L}_{\bar{d}g\bar{d}} = \bar{d}_i\sqrt{2}g_3\left(\tilde{D}_i^R P_L - \tilde{D}_i^L P_R\right)\Lambda_G, \quad (13)$$

$$\mathcal{L}_{\bar{u}dH} = \bar{u}_i\left(Y_{u,i}H_u^+ P_L + Y_{d,j}H_d^+ P_R\right)V_{ij}d_j, \quad (14)$$

$$\mathcal{L}_{\bar{\chi}^-d\bar{u}} = \left[(\tilde{H}_u^+ Y_{u,i}\tilde{U}_i^{R*} - g_2\tilde{W}^+\tilde{U}_i^{L*})P_L + Y_{d,j}\tilde{U}_i^{L*}\tilde{H}_d^+ P_R\right]V_{ij}d_j, \quad (15)$$

$$\begin{aligned} \mathcal{L}_{\bar{\chi}^0\bar{D}} &= \bar{d}_i\left\{ -\frac{1}{6}[2\sqrt{2}g_1\tilde{B}\tilde{D}_i^R + \sqrt{2}(2g_{YX} + 3g_X)\lambda_{\tilde{\chi}}\tilde{D}_i^R + 6Y_{d,i}\tilde{H}_d^0\tilde{D}_i^L]P_L \right. \\ &\quad \left. -\frac{1}{6}[6Y_{d,i}\tilde{D}_i^R\tilde{H}_d^0 + \sqrt{2}\tilde{D}_i^L(g_1\tilde{B} + g_{YX}\lambda_{\tilde{\chi}} - 3g_2\tilde{W}^0)]P_R \right\}. \quad (16) \end{aligned}$$

III. FORMULATION

At scale $\mu = O(m_b)$, the effective Hamiltonian of the flavor transition process $b \rightarrow s\gamma$ has the following form [33]:

$$\mathcal{H}_{eff}(b \rightarrow s\gamma) = -\frac{4G_F}{\sqrt{2}}V_{32}^*V_{33}\left[C_1Q_1^c + C_2Q_2^c + \sum_{i=3}^6 C_iQ_i + \sum_{i=7}^8 (C_iQ_i + \tilde{C}_i\tilde{Q}_i)\right], \quad (17)$$

and the operators are given by Refs. [34–36]:

$$\begin{aligned}
\mathcal{O}_1^c &= (\bar{s}_L \gamma_\mu T^a b_L)(\bar{c}_L \gamma^\mu T^a b_L), & \mathcal{O}_2^c &= (\bar{s}_L \gamma_\mu b_L)(\bar{c}_L \gamma^\mu b_L), \\
\mathcal{O}_3 &= (\bar{s}_L \gamma_\mu b_L) \sum_q (\bar{q} \gamma^\mu q), & \mathcal{O}_4 &= (\bar{s}_L \gamma_\mu T^a b_L) \sum_q (\bar{q} \gamma^\mu T^a q), \\
\mathcal{O}_5 &= (\bar{s}_L \gamma_\mu \gamma_\nu \gamma_\rho b_L) \sum_q (\bar{q} \gamma^\mu \gamma^\nu \gamma^\rho q), \\
\mathcal{O}_6 &= (\bar{s}_L \gamma_\mu \gamma_\nu \gamma_\rho T^a b_L) \sum_q (\bar{q} \gamma^\mu \gamma^\nu \gamma^\rho T^a q), \\
\mathcal{O}_7 &= e/g_3^2 m_b (\bar{s}_L \sigma_{\mu\nu} b_R) F^{\mu\nu}, & \mathcal{O}_8 &= 1/g_3^2 m_b (\bar{s}_L \sigma_{\mu\nu} T^a b_R) G^{a,\mu\nu}, \\
\tilde{\mathcal{O}}_7 &= e/g_3^2 m_b (\bar{s}_R \sigma_{\mu\nu} b_L) F^{\mu\nu}, & \tilde{\mathcal{O}}_8 &= 1/g_3^2 m_b (\bar{s}_R \sigma_{\mu\nu} T^a b_L) G^{a,\mu\nu}.
\end{aligned} \tag{18}$$

Through the amplitudes of the Feynman diagrams involved in the process $b \rightarrow s\gamma$, we can extract the coefficients of these operators. Actually, when we calculate the branching ratio with formula presented in Ref. [33]:

$$\begin{aligned}
& BR(\bar{B} \rightarrow X_s \gamma)_{NP} \\
&= 10^{-4} \times \left\{ (3.36 \pm 0.23) + \frac{16\pi^2 a_{77}}{\alpha_s^2(\mu_b)} [|C_{7,NP}(\mu_{EW})|^2 + |\tilde{C}_{7,NP}(\mu_{EW})|^2] \right. \\
&+ \frac{16\pi^2 a_{88}}{\alpha_s^2(\mu_b)} [|C_{8,NP}(\mu_{EW})|^2 + |\tilde{C}_{8,NP}(\mu_{EW})|^2] \\
&+ \frac{4\pi}{\alpha_s(\mu_b)} \text{Re} [a_7 C_{7,NP}(\mu_{EW}) + a_8 C_{8,NP}(\mu_{EW}) \\
&+ \left. \frac{4\pi a_{78}}{\alpha_s(\mu_b)} (C_{7,NP}(\mu_{EW}) C_{8,NP}(\mu_{EW}) + \tilde{C}_{7,NP}(\mu_{EW}) \tilde{C}_{8,NP}(\mu_{EW}))] \right\}, \tag{19}
\end{aligned}$$

only the coefficients of $\mathcal{O}_{7,8}$ and $\tilde{\mathcal{O}}_{7,8}$ are needed. In Eq.(19), the first term is the SM prediction, and $C_{7,NP}(\mu_{EW})$, $C_{8,NP}(\mu_{EW})$, $\tilde{C}_{7,NP}(\mu_{EW})$ and $\tilde{C}_{8,NP}(\mu_{EW})$ indicate Wilson coefficients at electroweak scale. In this representation, the effect evolved to the hadron scale $\mu \sim m_b$ has been included in the coefficients $a_{7,8,77,88,78}$. The numerical values of these coefficients are shown in Table I.

TABLE I: Numerical values for the coefficients $a_{7,8,77,88,78}$ at electroweak scale.

a_7	a_8	a_{77}	a_{88}	a_{78}
$-7.184 + 0.612i$	$-2.225 - 0.557i$	4.743	0.789	$2.454 - 0.884i$

A. Using MIA to calculate $b \rightarrow s\gamma$ in $U(1)_X$ SSM

The self-energy Feynman diagrams under the $U(1)_X$ SSM are obtained by MIA in Fig. 1. To obtain the branching ratio, we research one-loop diagrams in Fig. 1. To obtain triangle

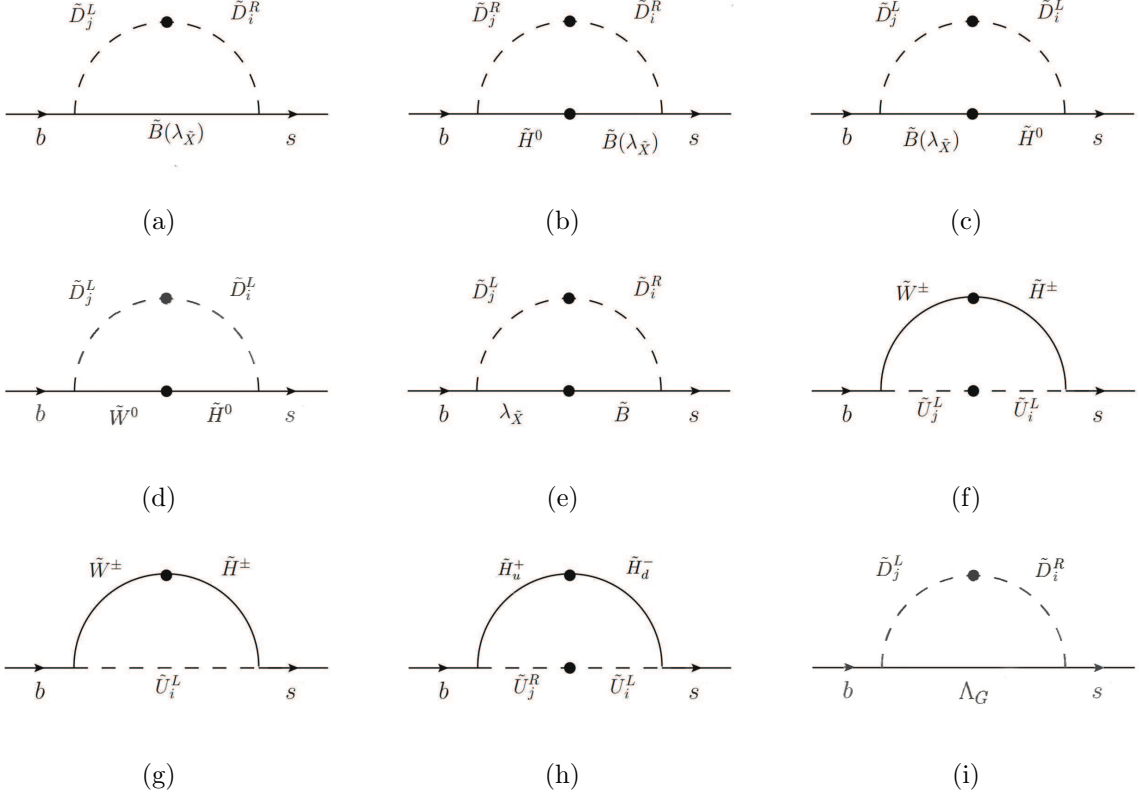


FIG. 1: Self-energy Feynman diagrams for $b \rightarrow s\gamma$ in the MIA.

diagrams, the photon should be attached to all inner lines with electric charge. In this case, the coefficients of \mathcal{O}_7 and $\tilde{\mathcal{O}}_7$ can be extracted from the amplitudes of these diagrams of $b \rightarrow s\gamma$. Similarly, the coefficients of \mathcal{O}_8 and $\tilde{\mathcal{O}}_8$ can be obtained from the diagrams of $b \rightarrow sg$ with gluons attached to all the inner lines with color charge. We give the following two basic functions:

$$f(x, y, z) = -\frac{i}{16\pi^2} \left[\frac{x \log x}{(x-y)(x-z)} - \frac{y \log y}{(y-x)(y-z)} - \frac{z \log z}{(z-x)(z-y)} \right], \quad (20)$$

$$g(x, y, z, t) = \frac{1}{z-t} \left(f(x, y, z) - f(x, y, t) \right). \quad (21)$$

1. The one-loop contributions from $\tilde{B}(\lambda_{\tilde{X}})-\tilde{D}_j^L-\tilde{D}_i^R$ ($i = 2, j = 3$).

$$C_7^1(\tilde{D}_j^L, \tilde{D}_i^R, \tilde{B}) = \frac{1}{216} \frac{T_d^{ij} v \cos \beta}{\mathcal{A} m_b \Lambda^3} g_3^2 g_1^2 \sqrt{x_1} I_1(x_1, x_{\tilde{D}_j^L}, x_{\tilde{D}_i^R}), \quad (22)$$

$$C_7^2(\tilde{D}_j^L, \tilde{D}_i^R, \lambda_{\tilde{X}}) = \frac{1}{432} \frac{T_d^{ij} v \cos \beta}{\mathcal{A} m_b \Lambda^3} g_3^2 (2g_{YX}^2 + 3g_{YX}g_X) \sqrt{x_{\lambda_{\tilde{X}}}} I_1(x_{\lambda_{\tilde{X}}}, x_{\tilde{D}_j^L}, x_{\tilde{D}_i^R}), \quad (23)$$

$$C_8^1(\tilde{D}_j^L, \tilde{D}_i^R, \tilde{B}) = \frac{1}{216} \frac{T_d^{ij} v \cos \beta}{\mathcal{A} m_b \Lambda^3} g_3^2 g_1^2 \sqrt{x_1} I_1(x_1, x_{\tilde{D}_j^L}, x_{\tilde{D}_i^R}), \quad (24)$$

$$C_8^2(\tilde{D}_j^L, \tilde{D}_i^R, \lambda_{\tilde{X}}) = \frac{1}{432} \frac{T_d^{ij} v \cos \beta}{\mathcal{A} m_b \Lambda^3} g_3^2 (2g_{YX}^2 + 3g_{YX}g_X) \sqrt{x_{\lambda_{\tilde{X}}}} I_1(x_{\lambda_{\tilde{X}}}, x_{\tilde{D}_j^L}, x_{\tilde{D}_i^R}), \quad (25)$$

in which, m stands for the particle mass, with $x = \frac{m^2}{\Lambda^2}$. The coefficient \mathcal{A} is equal to $\frac{1}{G_{FV_{32}^* V_{33}}}$ and Λ represents the energy scale. The function $I_1(x, y, z)$ is

$$I_1(x, y, z) = -\left(\frac{z}{2} \frac{\partial^2}{\partial z^2} + \frac{y}{2} \frac{\partial^2}{\partial y^2} + \frac{\partial}{\partial z} + y \frac{\partial^2}{\partial y \partial z}\right) f(x, y, z). \quad (26)$$

2. The one-loop contributions from $\tilde{B}(\lambda_{\tilde{X}})-\tilde{H}^0-\tilde{D}_j^R-\tilde{D}_i^R$ ($i = 2, j = 3$).

Figs 1(b)-1(e) are all computed with the same method of coefficients and the functions required in the process, so here we take Fig. 1(b) as an example.

$$C_7^3(\tilde{D}_j^R, \tilde{D}_i^R, \tilde{B}, \tilde{H}^0) = \frac{\sqrt{2} m_s \Delta_{ij}^{RR}(\tilde{D})}{72 \mathcal{A} m_b \Lambda^4} g_3^2 g_1^2 \tan \beta \sqrt{x_1 x_{\mu'_H}} I_2(x_1, x_{\tilde{D}_j^R}, x_{\tilde{D}_i^R}, x_{\mu'_H}), \quad (27)$$

$$C_7^4(\tilde{D}_j^R, \tilde{D}_i^R, \lambda_{\tilde{X}}, \tilde{H}^0) = \frac{\sqrt{2} m_s \Delta_{ij}^{RR}(\tilde{D})}{288 \mathcal{A} m_b \Lambda^4} g_3^2 (2g_{YX} + 3g_X)(g_{YX} + g_X) \\ \times \tan \beta \sqrt{2x_{\lambda_{\tilde{X}}} x_{\mu'_H}} I_2(x_{\lambda_{\tilde{X}}}, x_{\tilde{D}_j^R}, x_{\tilde{D}_i^R}, x_{\mu'_H}), \quad (28)$$

$$C_8^3(\tilde{D}_j^R, \tilde{D}_i^R, \tilde{B}, \tilde{H}^0) = \frac{\sqrt{2} m_s \Delta_{ij}^{RR}(\tilde{D})}{72 \mathcal{A} m_b \Lambda^4} g_3^2 g_1^2 \tan \beta \sqrt{x_1 x_{\mu'_H}} I_2(x_1, x_{\tilde{D}_j^R}, x_{\tilde{D}_i^R}, x_{\mu'_H}), \quad (29)$$

$$C_8^4(\tilde{D}_j^R, \tilde{D}_i^R, \lambda_{\tilde{X}}, \tilde{H}^0) = \frac{\sqrt{2} m_s \Delta_{ij}^{RR}(\tilde{D})}{288 \mathcal{A} m_b \Lambda^4} g_3^2 (2g_{YX} + 3g_X)(g_{YX} + g_X) \\ \times \tan \beta \sqrt{2x_{\lambda_{\tilde{X}}} x_{\mu'_H}} I_2(x_{\lambda_{\tilde{X}}}, x_{\tilde{D}_j^R}, x_{\tilde{D}_i^R}, x_{\mu'_H}), \quad (30)$$

in which, $\mu'_H = \frac{\lambda_H v_S}{\sqrt{2}} + \mu$ and $x_{\mu'_H} = \frac{\mu'^2_H}{\Lambda^2}$. The function $I_2(x, y, z, t)$ is

$$I_2(x, y, z, t) = -\left[\frac{z}{2} \frac{\partial^2}{\partial z^2} + \frac{y}{2} \frac{\partial^2}{\partial y^2} + \frac{\partial}{\partial z} + y \frac{\partial^2}{\partial y \partial z}\right] g(x, y, z, t). \quad (31)$$

3. The one-loop contributions from $\tilde{H}^\pm-\tilde{W}^\pm-\tilde{U}_j^L-\tilde{U}_i^L$.

$$C_7^5(\tilde{U}_j^L, \tilde{U}_i^L, \tilde{H}^\pm, \tilde{W}^\pm) = \frac{\sqrt{2}}{4} \sum_{i,j=1}^3 \frac{m_s \Delta_{ij}^{LL}(\tilde{U})}{\mathcal{A} m_b \Lambda^3} V_{2j}^* V_{3i} g_3^2 g_2 \left\{ \sqrt{x_2} I_3(x_{\mu'_H}, x_{\tilde{U}_j^L}, x_{\tilde{U}_i^L}, x_2) \right. \\ \left. + x_2 \sqrt{x_{\mu'_H}} \tan \beta I_4(x_{\mu'_H}, x_{\tilde{U}_j^R}, x_{\tilde{U}_i^R}, x_2) \right\}, \quad (32)$$

$$C_7^6(\tilde{U}_j^L, \tilde{U}_i^L, \tilde{H}^\pm, \tilde{W}^\pm) = \frac{\sqrt{2}}{6} \sum_{i,j=1}^3 \frac{m_s \Delta_{ij}^{LL}(\tilde{U})}{\mathcal{A} v m_b \Lambda^3} V_{2j}^* V_{3i} g_3^2 g_2 \left\{ \sqrt{x_2} I_3(x_{\mu'_H}, x_{\tilde{U}_j^L}, x_{\tilde{U}_i^L}, x_2) \right. \\ \left. + x_2 \sqrt{x_{\mu'_H}} \tan \beta I_2(x_{\mu'_H}, x_{\tilde{U}_j^L}, x_{\tilde{U}_i^L}, x_2) \right\}, \quad (33)$$

$$C_8^5(\tilde{U}_j^L, \tilde{U}_i^L, \tilde{H}^\pm, \tilde{W}^\pm) = \frac{\sqrt{2}}{6} \sum_{i,j=1}^3 \frac{m_s \Delta_{ij}^{LL}(\tilde{U})}{\mathcal{A} v m_b \Lambda^3} V_{2j}^* V_{3i} g_3^3 g_2 \left\{ \sqrt{x_2} I_3(x_{\mu'_H}, x_{\tilde{U}_j^L}, x_{\tilde{U}_i^L}, x_2) \right. \\ \left. + x_2 \sqrt{x_{\mu'_H}} \tan \beta I_2(x_{\mu'_H}, x_{\tilde{U}_j^L}, x_{\tilde{U}_i^L}, x_2) \right\}. \quad (34)$$

The functions $I_3(x, y, z, t)$ and $I_4(x, y, z, t)$ are

$$I_3(x, y, z, t) = - \left[1 + 2y \frac{\partial}{\partial y} + 2z \frac{\partial}{\partial z} + \frac{y^2}{2} \frac{\partial^2}{\partial y^2} + \frac{z^2}{2} \frac{\partial^2}{\partial z^2} + yz \frac{\partial^2}{\partial y \partial z} \right] g(x, y, z, t), \quad (35)$$

$$I_4(x, y, z, t) = \left[\frac{\partial}{\partial y} + 2 \frac{\partial}{\partial z} + \frac{y}{2} \frac{\partial^2}{\partial y^2} + \frac{z}{2} \frac{\partial^2}{\partial z^2} + y \frac{\partial^2}{\partial y \partial z} \right] g(x, y, z, t). \quad (36)$$

Similar to the third case, C_7^7, C_7^8, C_8^6 can be extracted from Fig. 1(h), and calculation process and form are the same as those of C_7^5, C_7^6, C_8^5 . We don't repeat them here.

4. The one-loop contributions from $\tilde{H}^\pm - \tilde{W}^\pm - \tilde{U}_i^L$.

$$C_7^7(\tilde{U}_i^L, \tilde{H}^\pm, \tilde{W}^\pm) = \frac{\sqrt{2}}{4} \sum_{i=1}^3 \frac{m_s}{\mathcal{A} v m_b \Lambda} V_{2i}^* V_{3i} g_3^2 g_2 \left\{ x_2 \sqrt{x_{\mu'_H}} \tan \beta I_5(x_{\tilde{U}_i^L}, x_2, x_{\mu'_H}) \right. \\ \left. + \sqrt{x_2} I_6(x_{\tilde{U}_i^L}, x_2, x_{\mu'_H}) \right\}, \quad (37)$$

$$C_7^8(\tilde{U}_i^L, \tilde{H}^\pm, \tilde{W}^\pm) = \frac{\sqrt{2}}{6} \sum_{i=1}^3 \frac{m_s}{\mathcal{A} v m_b \Lambda} V_{2i}^* V_{3i} g_3^2 g_2 \left\{ x_2 \sqrt{x_{\mu'_H}} \tan \beta I_7(x_{\mu'_H}, x_2, x_{\tilde{U}_i^L}) \right. \\ \left. - \sqrt{x_2} I_8(x_{\mu'_H}, x_2, x_{\tilde{U}_i^L}) \right\}, \quad (38)$$

$$C_8^6(\tilde{U}_i^L, \tilde{H}^\pm, \tilde{W}^\pm) = \frac{\sqrt{2}}{6} \sum_{i=1}^3 \frac{m_s}{\mathcal{A} v m_b \Lambda} V_{2i}^* V_{3i} g_3^3 g_2 \left\{ x_2 \sqrt{x_{\mu'_H}} \tan \beta I_7(x_{\mu'_H}, x_2, x_{\tilde{U}_i^L}) \right. \\ \left. - \sqrt{x_2} I_8(x_{\mu'_H}, x_2, x_{\tilde{U}_i^L}) \right\}. \quad (39)$$

The functions $I_5(x, y, z), I_6(x, y, z), I_7(x, y, z)$ and $I_8(x, y, z)$ are

$$I_5(x, y, z) = \left[\frac{\partial}{\partial y} + 2 \frac{\partial}{\partial z} + \frac{y}{2} \frac{\partial^2}{\partial y^2} + \frac{z}{2} \frac{\partial^2}{\partial z^2} + y \frac{\partial^2}{\partial y \partial z} \right] f(x, y, z), \quad (40)$$

$$I_6(x, y, z) = \left[1 + 2y \frac{\partial}{\partial y} + 2z \frac{\partial}{\partial z} + \frac{y^2}{2} \frac{\partial^2}{\partial y^2} + \frac{z^2}{2} \frac{\partial^2}{\partial z^2} + yz \frac{\partial^2}{\partial y \partial z} \right] f(x, y, z), \quad (41)$$

$$I_7(x, y, z) = \left[\frac{\partial}{\partial z} + \frac{z}{2} \frac{\partial^2}{\partial z^2} \right] f(x, y, z), \quad I_8(x, y, z) = \left[1 + z \frac{\partial}{\partial z} \right] f(x, y, z). \quad (42)$$

5. The one-loop contributions from Λ_G - \tilde{D}_j^L - \tilde{D}_i^R ($i = 2, j = 3$).

$$C_7^9(\tilde{D}_j^L, \tilde{D}_i^R, \Lambda_G) = -\frac{1}{48} \frac{T_d^{ij} v \cos \beta}{\mathcal{A} m_b \Lambda^3} g_3^4 \sqrt{x_{\Lambda_G}} I_1(x_{\Lambda_G}, x_{\tilde{D}_j^L}, x_{\tilde{D}_i^R}), \quad (43)$$

$$C_8^7(\tilde{D}_j^L, \tilde{D}_i^R, \Lambda_G) = -\frac{1}{16} \frac{T_d^{ij} v \cos \beta}{\mathcal{A} m_b \Lambda^3} g_3^5 \sqrt{x_{\Lambda_G}} I_7(x_{\tilde{D}_j^L}, x_{\tilde{D}_i^R}, x_{\Lambda_G}), \quad (44)$$

$$C_8^8(\tilde{D}_j^L, \tilde{D}_i^R, \Lambda_G) = -\frac{1}{48} \frac{T_d^{ij} v \cos \beta}{\mathcal{A} m_b \Lambda^3} g_3^5 \sqrt{x_{\Lambda_G}} I_1(x_{\Lambda_G}, x_{\tilde{D}_j^L}, x_{\tilde{D}_i^R}). \quad (45)$$

According to the above procedure, we can get the coefficients of all the diagrams in Fig. 1. We add the coefficients of each diagram separately to obtain the Wilson coefficients, and import them into Eq.(19) to obtain the branching ratio.

B. Degenerate Result

Assuming that the masses of all the superparticles are almost degenerate, we are able to more intuitively analyze the factors affecting the flavor transition process $b \rightarrow s\gamma$. In other words, we give the one-loop results in the extreme case, where the masses for superparticles ($M_1, M_2, \mu'_H, M_{\Lambda_G}, M_{\lambda_{\tilde{\chi}}}, M_{\tilde{D}_L}, M_{\tilde{D}_R}, M_{\tilde{U}_L}, M_{\tilde{U}_R}, M_{BB'}$) are equal to M_{SUSY} :

$$\begin{aligned} |M_1| &= |M_2| = |\mu'_H| = |M_{\Lambda_G}| = |M_{\lambda_{\tilde{\chi}}}| = |M_{BB'}| \\ &= M_{\tilde{D}_L} = M_{\tilde{D}_R} = M_{\tilde{U}_L} = M_{\tilde{U}_R} = M_{SUSY}. \end{aligned} \quad (46)$$

The functions I_i ($i = 1 \dots 11$), $\Delta_{ij}^{AB}(\tilde{Q})(A, B = R, L)$, T_d^{ij} and T_u^{ij} are much simplified as

$$\begin{aligned} I_1(1, 1, 1) &= \frac{i}{192\pi^2}, & I_2(1, 1, 1) &= \frac{i}{192\pi^2}, & I_3(1, 1, 1, 1) &= -\frac{i}{320\pi^2}, \\ I_4(1, 1, 1, 1) &= -\frac{i}{480\pi^2}, & I_5(1, 1, 1, 1) &= \frac{i}{480\pi^2}, & I_6(1, 1, 1, 1) &= \frac{i}{320\pi^2}, \\ I_7(1, 1, 1, 1) &= -\frac{i}{480\pi^2}, & I_8(1, 1, 1) &= -\frac{i}{192\pi^2}, & I_9(1, 1, 1) &= -\frac{i}{64\pi^2}, \\ I_{10}(1, 1, 1) &= \frac{i}{192\pi^2}, & I_{11}(1, 1, 1) &= -\frac{i}{48\pi^2}, \end{aligned} \quad (47)$$

$$\begin{aligned} \Delta_{ij}^{LL}(\tilde{D}) &= M_{SUSY}^2 \delta_{ij}^{LL}(\tilde{D}), & \Delta_{ij}^{RR}(\tilde{D}) &= M_{SUSY}^2 \delta_{ij}^{RR}(\tilde{D}), & \Delta_{ij}^{LL}(\tilde{U}) &= M_{SUSY}^2 \delta_{ij}^{LL}(\tilde{U}), \\ T_d^{ij} &= M_{SUSY} \delta_{T_d}^{ij}, & T_u^{ij} &= M_{SUSY} \delta_{T_u}^{ij}. \end{aligned} \quad (48)$$

To simplify the study, we suppose that the used matrices are symmetric, for example $T_d^{ij} = T_d^{ji}$.

Then, we obtain the much simplified one-loop results of C_7 and C_8

$$\begin{aligned}
C_7 = & \frac{iAg_3^2}{2304\pi^2 M_{SUSY}^2} \left\{ \frac{\tan\beta}{15} \delta_{23}^{RR}(\tilde{D}) \left((3g_X^2 + g_X g_{YX} - 2g_{YX}^2) \text{sign}[M_{\lambda_{\tilde{X}}}] \mu'_H - 2g_1^2 \text{sign}[M_1 \mu'_H] \right) \right. \\
& + \frac{\tan\beta}{15} \frac{m_s}{m_b} \delta_{23}^{LL}(\tilde{D}) \left(3g_2^2 \text{sign}[M_2 \mu'_H] - (g_X g_{YX} + g_{YX}^2) \text{sign}[M_{\lambda_{\tilde{X}}}] \mu'_H - g_1^2 \text{sign}[M_1 \mu'_H] \right) \\
& + \frac{v \cos\beta \delta_{T_d}^{23}}{180m_b} \left(10g_1^2 \text{sign}[M_1] + (15g_X g_{YX} + 10g_{YX}^2) \text{sign}[M_{\lambda_{\tilde{X}}}] - 8g_1 g_{YX} \text{sign}[M_{\lambda_{\tilde{X}}} M_1 M_{BB'}] \right. \\
& \left. - 45g_3^2 \text{sign}[M_{\Lambda_G}] \right) + \frac{\sqrt{2} M_{SUSY} m_s}{v m_b} g_2 \left(2 \tan\beta \text{sign}[\mu'_H] - \text{sign}[M_2] \right) \sum_{l,n=1}^3 V_{2n}^* V_{3l} \delta_{ln}^{LL}(\tilde{U}) \\
& \left. - \frac{22m_s \text{sign}[\mu'_H]}{5m_b v \cos\beta} \sum_{i,j=1}^3 V_{2i}^* V_{3j} m_{u_j} \delta_{T_u}^{ji} \right\}, \tag{49}
\end{aligned}$$

$$\begin{aligned}
C_8 = & \frac{iAg_3^3}{240\pi^2 M_{SUSY}^2} \left\{ \frac{\tan\beta}{12} \delta_{23}^{RR}(\tilde{D}) \left((3g_X^2 + g_X g_{YX} - 2g_{YX}^2) \text{sign}[M_{\lambda_{\tilde{X}}}] \mu'_H - 2g_1^2 \text{sign}[M_1 \mu'_H] \right) \right. \\
& + \frac{\tan\beta}{12} \frac{m_s}{m_b} \delta_{23}^{LL}(\tilde{D}) \left(3g_2^2 \text{sign}[M_2 \mu'_H] - (g_X g_{YX} + g_{YX}^2) \text{sign}[M_{\lambda_{\tilde{X}}}] \mu'_H - g_1^2 \text{sign}[M_1 \mu'_H] \right) \\
& + \frac{v \cos\beta \delta_{T_d}^{23}}{144m_b} \left(10g_1^2 \text{sign}[M_1] + (15g_X g_{YX} + 10g_{YX}^2) \text{sign}[M_{\lambda_{\tilde{X}}}] - 8g_1 g_{YX} \text{sign}[M_{\lambda_{\tilde{X}}} M_1 M_{BB'}] \right. \\
& \left. - 60g_3^2 \text{sign}[M_{\Lambda_G}] \right) + \frac{\sqrt{2} M_{SUSY} m_s}{4v m_b} g_2 \left(\text{sign}[M_2] - 4 \tan\beta \text{sign}[\mu'_H] \right) \sum_{l,n=1}^3 V_{2n}^* V_{3l} \delta_{ln}^{LL}(\tilde{U}) \\
& \left. - \frac{2m_s \text{sign}[\mu'_H]}{m_b v \cos\beta} \sum_{i,j=1}^3 V_{2i}^* V_{3j} m_{u_j} \delta_{T_u}^{ji} \right\}. \tag{50}
\end{aligned}$$

It can be found that $\text{sign}[M_1]$, $\text{sign}[M_2]$, $\text{sign}[M_{\lambda_{\tilde{X}}}]$, $\text{sign}[\mu'_H]$, $\text{sign}[M_G]$ and $\text{sign}[M_{BB'}]$ have a certain impact on the corrections of C_7 and C_8 . According to $1 > g_X > g_{YX} > 0$, we assume $\text{sign}[M_1] = \text{sign}[M_{\lambda_{\tilde{X}}}] = \text{sign}[\mu'_H] = \text{sign}[M_2] = \text{sign}[M_G] = \text{sign}[M_{BB'}] = 1$, and get the larger values of C_7 and C_8

$$\begin{aligned}
C_7 = & \frac{iAg_3^2}{2304\pi^2 M_{SUSY}^2} \left\{ \frac{\tan\beta}{15} \delta_{23}^{RR}(\tilde{D}) (3g_X^2 + g_X g_{YX} - 2g_{YX}^2 - 2g_1^2) + \frac{\tan\beta}{15} \frac{m_s}{m_b} \delta_{23}^{LL}(\tilde{D}) \right. \\
& \times (3g_2^2 - g_X g_{YX} - g_{YX}^2 - g_1^2) + \frac{v \cos\beta \delta_{T_d}^{23}}{180m_b} (10g_1^2 + 15g_X g_{YX} + 10g_{YX}^2 - 8g_1 g_{YX} - 45g_3^2) \\
& \left. + \frac{\sqrt{2} m_s M_{SUSY}}{m_b v} g_2 (2 \tan\beta - 1) \sum_{l,n=1}^3 V_{2n}^* V_{3l} \delta_{ln}^{LL}(\tilde{U}) - \frac{22m_s}{5m_b v \cos\beta} \sum_{i,j=1}^3 V_{2i}^* V_{3j} m_{u_j} \delta_{T_u}^{ji} \right\}, \tag{51}
\end{aligned}$$

$$\begin{aligned}
C_8 = & \frac{iAg_3^3}{240\pi^2 M_{SUSY}^2} \left\{ \frac{\tan\beta}{12} \delta_{23}^{RR}(\tilde{D})(3g_X^2 + g_X g_{YX} - 2g_{YX}^2 - 2g_1^2) + \frac{\tan\beta}{12} \frac{m_s}{m_b} \delta_{23}^{LL}(\tilde{D}) \right. \\
& \times (3g_2^2 - g_X g_{YX} - g_{YX}^2 - g_1^2) + \frac{v \cos\beta \delta_{T_d}^{23}}{144m_b} (10g_1^2 + 15g_X g_{YX} + 10g_{YX}^2 - 8g_1 g_{YX} - 60g_3^2) \\
& \left. + \frac{\sqrt{2}m_s M_{SUSY}}{4m_b v} g_2 (1 - 4 \tan\beta) \sum_{l,n=1}^3 V_{2n}^* V_{3l} \delta_{ln}^{LL}(\tilde{U}) - \frac{2m_s}{m_b v \cos\beta} \sum_{i,j=1}^3 V_{2i}^* V_{3j} m_{u_j} \delta_{T_u}^{ji} \right\}. \quad (52)
\end{aligned}$$

To determine the sensitive parameters affecting the branching ratio more clearly and intuitively, similar method is used to derive \tilde{C}_7 and \tilde{C}_8 in Eq.(19). Then in combination with the degenerate results in Eq.(51), Eq.(52) and Eq.(48), we set $M_{SUSY} = \mu'_H$, $g_{YX} = 0.1$, $g_X = 0.5$, $\Delta_{23}^{RR}(\tilde{D}) = \Delta_{23}^{LL}(\tilde{D}) = 1 \times 10^4 \text{ GeV}^2$, $\Delta_{ij}^{LL}(\tilde{U}) = 4.2 \times 10^4 \text{ GeV}^2$ ($i \neq j$ and $i, j = 1, 2, 3$) and $\Delta_{ii}^{LL}(\tilde{U}) = 5 \times 10^6 \text{ GeV}^2$ ($i = 1, 2, 3$) to obtain the following figures:

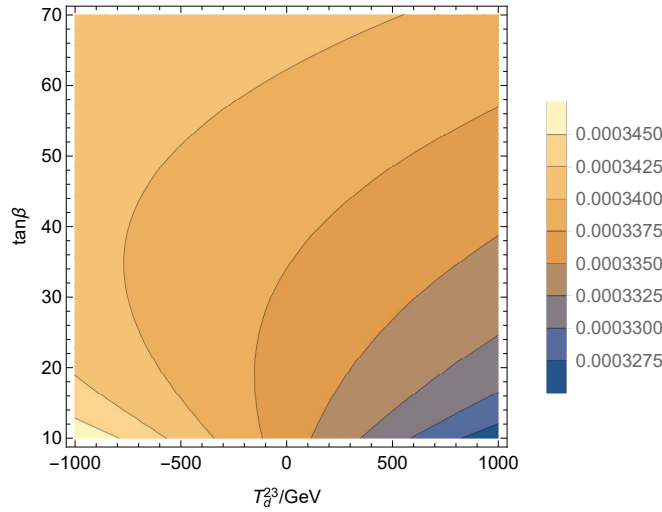


FIG. 2: With $T_u^{23} = -650 \text{ GeV}$ and $\mu = 1000 \text{ GeV}$, the effects of $\tan\beta$ and T_d^{23} on $Br(\bar{B} \rightarrow X_s \gamma)$. The x-axis denotes the range of T_d^{23} is from -1000 GeV to 1000 GeV , and the y-axis represents $10 < \tan\beta < 70$. The different colors of the rightmost icon correspond to the values of $Br(\bar{B} \rightarrow X_s \gamma)$.

Combined with Fig. 2 and Fig. 3, it can be seen that $\tan\beta$, μ , T_d^{23} and T_u^{23} have a significant impact on the results. In Fig. 2, we can see that $Br(\bar{B} \rightarrow X_s \gamma)$ increases as the $\tan\beta$ increases. The reason can be found in Eq.(51) and Eq.(52). $\tan\beta$ is almost always in the numerator, so it is proportional to the result. When $\tan\beta = 40$ and $T_d^{23} = -600 \text{ GeV}$, $Br(\bar{B} \rightarrow X_s \gamma)$ reaches 3.4×10^{-4} . Compared to the influence of T_d^{23} , $\tan\beta$ obviously has stronger influence. In our hypothesis, M_{SUSY} is equal to μ'_H , and μ is proportional

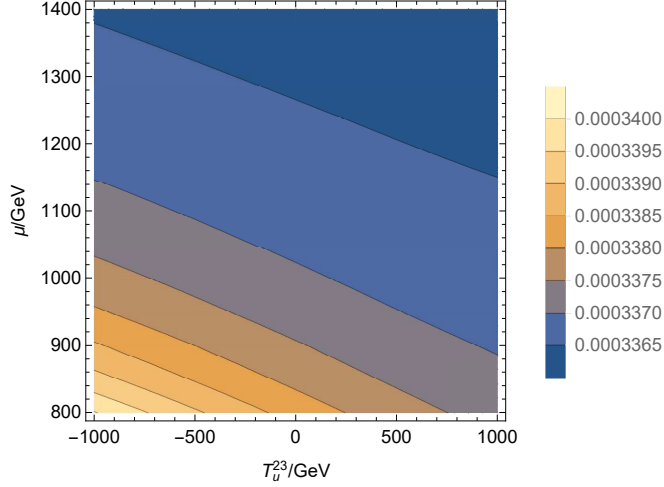


FIG. 3: With $T_d^{23} = 600$ GeV and $\tan\beta = 50$, the effects of μ and T_u^{23} on $Br(\bar{B} \rightarrow X_s\gamma)$. The x-axis denotes the range of T_u^{23} is from -1000 GeV to 1000 GeV, and the y-axis represents 800 GeV $< \mu < 1400$ GeV. The different colors of the rightmost icon correspond to the values of $Br(\bar{B} \rightarrow X_s\gamma)$.

to μ'_H . In Eq.(51) and Eq.(52), M_{SUSY} is inversely proportional to the result. Thus, μ should be inversely proportional to the result, which can be demonstrated in Fig. 3. When $\mu = 800$ GeV and $T_u^{23} = -730$ GeV, the branching ratio reaches 3.4×10^{-4} . And the influence of μ is greater than that of T_u^{23} . At the same time, as the values of FCNC sources $\Delta_{ij}^{LL}(\tilde{D})$, $\Delta_{ij}^{RR}(\tilde{D})$ and $\Delta_{ij}^{LL}(\tilde{U})$ go up, the result also grows. But they have gentle influence on the result, which is not shown here. In summary, we can get the sensitive parameters including $\tan\beta$, μ , T_d^{23} and T_u^{23} .

IV. NUMERICAL RESULTS

To study $Br(\bar{B} \rightarrow X_s\gamma)$, we consider the mass constraint for the Z' boson ($M_{Z'} > 5.1$ TeV) [37] from the latest Large Hadron Collider (LHC) data [38–44]. The constraints $M_{Z'}/g_X \geq 6$ TeV and $\tan\beta_\eta < 1.5$ are also taken into account. According to the research in Ref. [45], we take the mass of gluino more than 2 TeV. The parameters are used to make the scalar lepton masses larger than 700 GeV, and chargino masses larger than 1100 GeV, and the scalar quark masses greater than 2000 GeV. Ref. [46] and Ref. [47] discuss parameter space for $b \rightarrow s\gamma$ under various models, and in their data analysis the value of $\tan\beta$ is

relatively high. Considering that $U(1)_X$ S SM has more parameters and larger adjustment space of parameters, we tend to choose a large value of $\tan\beta$.

In this section, we discuss the numerical results of branching ratio with some assumptions. Other free parameters introduced in the $U(1)_X$ S SM are set to

$$g_X = 0.4, g_{YX} = 0.1, \lambda_H = 0.1, v_S = 3.5 \text{ TeV}, T_{u11} = T_{u22} = T_{u33} = 3 \text{ TeV},$$

$$M_1 = 1 \text{ TeV}, M_2 = 1.1 \text{ TeV}, M_{\lambda_{\tilde{X}}} = 1.4 \text{ TeV}, M_G = 2.1 \text{ TeV}, M_{BB'} = 0.8 \text{ TeV}.(53)$$

After roughly determining the sensitive parameters, in order to study the influence of parameters on $Br(\bar{B} \rightarrow X_s \gamma)$ better, we also need to study before degenerate. To show the numerical results clearly, we draw the relation diagrams and scatter diagrams of $Br(\bar{B} \rightarrow X_s \gamma)$ with the parameters of the $U(1)_X$ S SM. Fig. 4 shows the relationship between $\tan\beta$

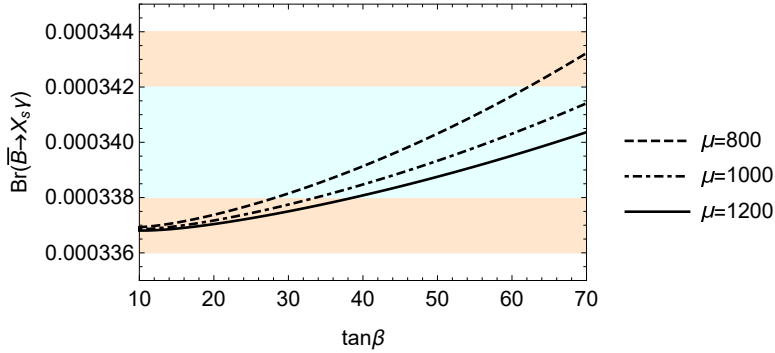


FIG. 4: $Br(\bar{B} \rightarrow X_s \gamma)$ versus $\tan\beta$ with $\Delta^{ij} = 3 \times 10^5 \text{ GeV}^2$.

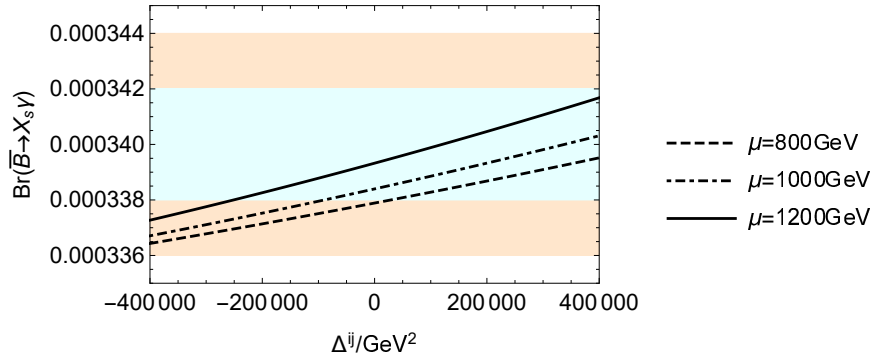


FIG. 5: $Br(\bar{B} \rightarrow X_s \gamma)$ versus Δ^{ij} with $\tan\beta = 60$.

and $Br(\bar{B} \rightarrow X_s \gamma)$, where $Br(\bar{B} \rightarrow X_s \gamma)$ increases with the enlarging $\tan\beta$. As the lines in the figure go from bottom to top, the value of μ decreases gradually. Meanwhile, under

the same $\tan\beta$, the smaller the μ is, the larger the value of $Br(\bar{B} \rightarrow X_s\gamma)$ is. This is the same as the conclusion of degenerate results. When the value of μ decreases, the influence of $\tan\beta$ gradually becomes more significant. Since the influences of some FCNC sources are small, we set $\Delta_{ij}^{LL}(\tilde{D})$, $\Delta_{ij}^{RR}(\tilde{D})$ and $\Delta_{ij}^{LL}(\tilde{U})$ to be equal in the drawing of the diagram, and their values are represented by $\Delta^{ij}(i \neq j)$, so as to get Fig. 5. The result is proportional to Δ^{ij} . When $\Delta^{ij} = 1.3 \times 10^5 \text{ GeV}^2$ and $\mu = 800 \text{ GeV}$, $Br(\bar{B} \rightarrow X_s\gamma)$ reaches 3.4×10^{-4} . Compared with the degenerate result, the influence degree of some parameters on the result has changed. For example, the effects of T_d^{23} and T_u^{23} are reduced in precise results. But Δ^{ij} , which have less effect on the degenerate result, have more effect here.

For more multidimensional analysis of sensitive parameters, we draw the scatter points in Figs. 6 - 8. Under the premise of current limit on flavor transition process $b \rightarrow s\gamma$, we select the parameter ranges as follows:

$$\begin{aligned} \tan\beta &= 10 \sim 70, & T_d^{23} &= -1000 \sim 1000 \text{ GeV}, \\ \mu &= 800 \sim 1300 \text{ GeV}, & \Delta^{ij} &= (-4.0 \sim 4.0) \times 10^5 \text{ GeV}^2. \end{aligned} \quad (54)$$

In Figs. 6 - 8, \blacklozenge mean the value of $Br(\bar{B} \rightarrow X_s\gamma)$ less than 3.37×10^{-4} , \blacktriangle mean $Br(\bar{B} \rightarrow X_s\gamma)$ in the range of 3.37×10^{-4} to 3.39×10^{-4} , \blacksquare show $3.39 \times 10^{-4} \leq Br(\bar{B} \rightarrow X_s\gamma)$.

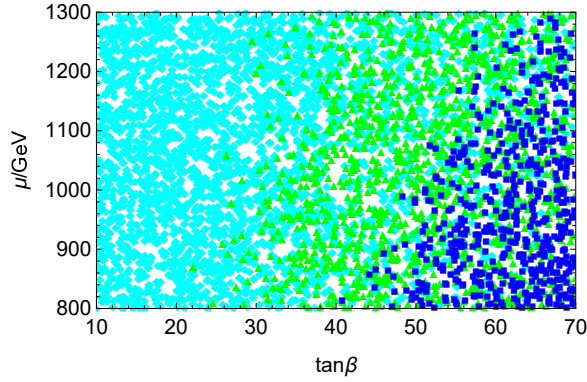


FIG. 6: The effects of $\tan\beta$ and μ on $Br(\bar{B} \rightarrow X_s\gamma)$.

Fig. 6 shows the relationship between $\tan\beta$ and μ , and it can be seen that the largest area is occupied by \blacklozenge . \blacksquare are mainly concentrated on the right side of the image and decrease with the increase of μ or the decrease of $\tan\beta$. When $\tan\beta$ is greater than 45, the result is easier to get to 3.40×10^{-4} . Moreover, the three markers \blacklozenge , \blacktriangle and \blacksquare have clear distribution boundaries, and $\tan\beta$ has a greater impact on the results.

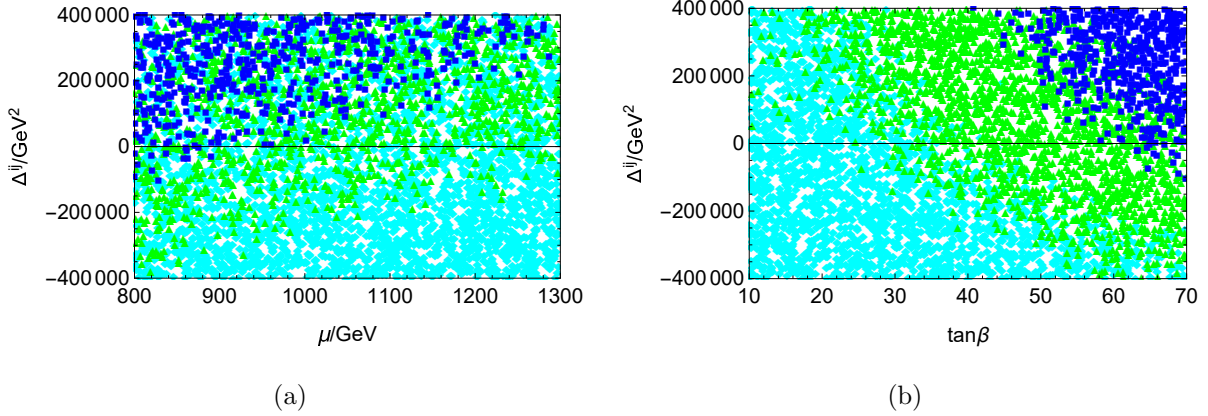


FIG. 7: The effects of μ and Δ^{ij} on $Br(\bar{B} \rightarrow X_s \gamma)$ (a); the effects of $\tan \beta$ and Δ^{ij} on $Br(\bar{B} \rightarrow X_s \gamma)$ (b).

Fig. 7(a) shows the relationship between μ and Δ^{ij} , and Fig. 7(b) is the relationship between $\tan \beta$ and Δ^{ij} . It can be further seen from the figure that $\tan \beta$ has more obvious influence than μ , because the distribution of midpoints in Fig. 7(a) is not as clear as that in Fig. 7(b). For example marker \blacklozenge , in Fig. 7(a), marker \blacklozenge are widely distributed. In contrast, the markers in Fig. 7(b) are mainly concentrated in the lower left part, and there is no marker \blacklozenge in the upper right part. Combining the two graphs, Δ^{ij} increase and so does the branching ratio. And when Δ^{ij} are greater than $-1 \times 10^{-5} \text{ GeV}^2$, it is easier to reach 3.40×10^{-4} . The relationship between T_d^{23} and $\tan \beta$ is shown in Fig. 8. It can be seen

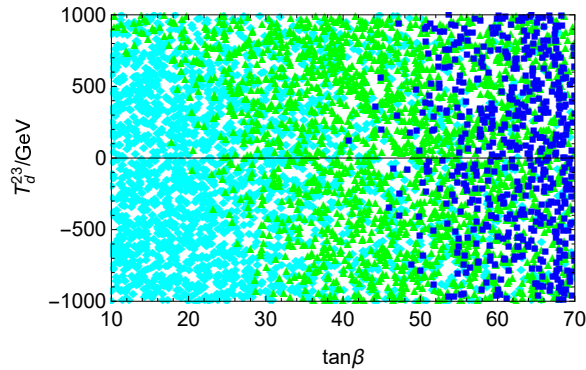


FIG. 8: The effect of $\tan \beta$ and T_d^{23} on $Br(\bar{B} \rightarrow X_s \gamma)$.

that the results increase with the enlarging T_d^{23} . However, when $\tan \beta$ increases to a certain extent, the influence of T_d^{23} turns weak gradually.

V. DISCUSSION AND CONCLUSION

The $U(1)_X$ SSM has new superfields including right-handed neutrinos $\hat{\nu}_i$ and three Higgs superfields $\hat{\eta}$, $\hat{\eta}'$, \hat{S} , and its local gauge group is $SU(3)_C \otimes SU(2)_L \otimes U(1)_Y \otimes U(1)_X$. As an interesting process of FCNC, the flavor transition process $b \rightarrow s\gamma$ is investigated by the MIA within the framework of the $U(1)_X$ SSM. With effective Hamiltonian method, we present the Wilson coefficients extracted from amplitudes corresponding to the concerned one-loop diagrams. Based on the analytical results, constraints on the parameters are given with the experimental data of $Br(\bar{B} \rightarrow X_s\gamma)$. From the data analysis, the flavor transition process $b \rightarrow s\gamma$ has relatively stricter restrictions on the quark flavor violation sources than most other parameters.

We take into account the constraint from the branching ratio. By MIA, we obtain simpler degenerate results. These results contribute to us to more intuitively determine sensitive parameters. It is convenient for subsequent numerical analysis. Through the multi-angle analysis of the values, it is found that the branching ratio is more dependent on the variables $\tan\beta$ and μ in the $U(1)_X$ SSM. Δ^{ij} are composed of quark flavor violation sources $\Delta_{ij}^{LL}(\tilde{D})$, $\Delta_{ij}^{RR}(\tilde{D})$ and $\Delta_{ij}^{LL}(\tilde{U})$, and the influence is also obvious. The effects of T_d^{23} and T_u^{23} are relatively insignificant. Parameters that are not graphed, such as g_X and g_{YX} , have gentle effects on the results. g_X , g_{YX} , g_1 , g_2 , and g_3 are the coupling constants. g_X and g_{YX} only appear in some part of analytical result. So the impact of g_X and g_{YX} is relatively small. Therefore, we can get the main sensitive parameters that are $\tan\beta$, μ and the FCNC sources Δ^{ij} . This work is conducive to further research on the $U(1)_X$ SSM and FCNC.

Acknowledgments

This work is supported by National Natural Science Foundation of China (NNSFC) (No. 12075074), Natural Science Foundation of Hebei Province (A2020201002, A202201022, A2022201017), Natural Science Foundation of Hebei Education Department (QN2022173), Post-graduate's Innovation Fund Project of Hebei University (HBU2023SS043), the youth top-notch talent support program of the Hebei Province.

Data Availability Statement: The data are available from the corresponding author

on reasonable request.

-
- [1] M. Ciuchini, G. Degrossi, P. Gambino and G. F. Giudice, Nucl. Phys. B **527** (1998) 21.
 - [2] P. Ciafaloni, A. Romanino and A. Strumia, Nucl. Phys. B **524** (1998) 361.
 - [3] F. Borzumati and C. Greub, Phys. Rev. D **58** (1998) 074004.
 - [4] S. Bertolini, F. Borzumati, A. Masiero and G. Ridolfi, Nucl. Phys. B **353** (1991) 591.
 - [5] R. Barbieri and G.F. Giudice, Phys. Lett. B **309** (1993) 86.
 - [6] F. Borzumati, C. Greub, T. Hurth and D. Wyler, Phys. Rev. D **62** (2000) 075005.
 - [7] S. Prelovsek and D. Wyler, Phys. Lett. B **500** (2001) 304.
 - [8] M. Causse and J. Orloff, Eur. Phys. J. C **23** (2002) 749.
 - [9] H.B. Zhang, G.H. Luo, T.F. Feng, S.M. Zhao, T.J. Gao and K.S. Sun, Mod. Phys. Lett. A **29** (2014) 1450196 [arXiv:1409.6837].
 - [10] M. Tanabashi, et al. (Particle Data Group), Phys. Rev. D **98** (2018) 030001.
 - [11] M. Misiak, et al., Phys. Rev. Lett. **114** (2015) 221801.
 - [12] M. Czakon, P. Fiedler, et al., JHEP **168** (2015) [arXiv:1503.01791].
 - [13] M. Misiak, et al., Phys. Rev. Lett. **98** (2007) 022002.
 - [14] M. Misiak and M. Steinhauser, Nucl. Phys. B **62** (2007) 764.
 - [15] K. Chetyrkin, M. Misiak and M. Munz, Phys. Lett. B **400** (1997) 206-219.
 - [16] C. Greub, T. Hurth and D. Wyler, Phys. Rev. D **54** (1996) 3350-3364.
 - [17] K. Adel and Y.P. Yao, Phys. Rev. D **49** (1994) 4945-4948.
 - [18] A. Ali and C. Greub, Phys. Lett. B **361** (1995) 146-154.
 - [19] J. Rosiek, Phys. Rev. D **41** (1990) 3464 [arXiv:hep-ph/9511250].
 - [20] S.M. Zhao, T.F. Feng, M.J. Zhang, et al., JHEP **02** (2020) 130 [arXiv:1905.11007].
 - [21] S.M. Zhao, L.H. Su, X.X. Dong, et al., JHEP **03** (2022) 101 [arXiv:2107.03571].
 - [22] F. Gabbiani, E. Gabrielli, A. Masiero, et al., Nucl. Phys. B **477** (1996) 321.
 - [23] E. Arganda, M.J. Herrero, and R. Morales, et al., JHEP **03** (2016) 055.
 - [24] E. Arganda, M.J. Herrero and X. Marcano, et al., Phys. Rev. D **95** (2017) 095029.
 - [25] M.J. Herrero, X. Marcano and R. Morales, et al., Eur. Phys. J. C **78** (2018) 815.
 - [26] A. Dedes, M. Paraskevas and J. Rosiek, et al., JHEP **1506** (2015) 151.
 - [27] G. Belanger, J.D. Silva and H.M. Tran, Phys. Rev. D **95** (2017) 115017.

- [28] V. Barger, P.F. Perez and S. Spinner, Phys. Rev. Lett. **102** (2009) 181802.
- [29] P.H. Chankowski, S. Pokorski and J. Wagner, Eur. Phys. J. C **47** (2006) 187.
- [30] J.L. Yang, T.F. Feng and S.M. Zhao, et al., Eur. Phys. J. C **78** (2018) 714.
- [31] B. Yan, S.M. Zhao and T.F. Feng, Nucl. Phys. B **975** (2022) 115671.
- [32] T.T. Wang, S.M. Zhao and X.X. Dong, et al., JHEP **04** (2022) 122.
- [33] E. Lunghi and J. Matias, JHEP **04** (2007) 058.
- [34] T.F. Feng, Y.L. Yan, H.B. Zhang, et al., Phys. Rev. D **92** (2015) 055024.
- [35] C. Bobeth, M. Misiak and J. Urban, Nucl. Phys. B **574** (2000) 291-330.
- [36] W. Altmannshofer, P. Balll, A. Bharucha, et al., JHEP **01** (2009) 019.
- [37] The ATLAS Collaboration, Phys. Lett. B **796** (2019) 68.
- [38] M. Endo, K. Hamaguchi, S. Iwamoto, et al., JHEP **07** (2021) 075.
- [39] M. Chakraborti, L. Roszkowski and S. Trojanowski, JHEP **05** (2021) 252. [arXiv:2104.04458].
- [40] F. Wang, L. Wu, Y. Xiao, et al., Nucl. Phys. B. **970** (2021) 115486 [arXiv:2104.03262].
- [41] P. Cox, C.C. Han, and T.T. Yanagida, Phys. Rev. D. **104** (2021) 075035 [arXiv:2104.03290].
- [42] M.V. Beekveld, W. Beenakker, M. Schutten, et al., SciPost Phys. **11** (2021) 049. [arXiv:2104.03245].
- [43] M. Chakraborti, S. Heinemeyer and I. Saha, Eur. Phys. J. C. **81** (2021) 1114. [arXiv:2104.03287].
- [44] P. Athron, C. Balazs, D.H.J. Jacob, et al., JHEP **09** (2021) 080 [arXiv:2104.03691].
- [45] G. Aad et al. [ATLAS], JHEP **10** (2020) 062.
- [46] F. Mahmoudi, JHEP **12** (2007) 026.
- [47] Keith A. Olive and L. Velasco-Sevilla, JHEP **05** (2008) 052.